THE ASTROPHYSICAL JOURNAL, 315:580–587, 1987 April 15

VRO 42.05.01: A SUPERNOVA REMNANT REENERGIZING AN INTERSTELLAR CAVITY

S. PINEAULT
Département de physique and Observatoire du Mont Mégantic, Université Laval, Québec
T. L. LANDECKER
Dominion Radio Astrophysical Observatory, National Research Council of Canada, Penticton, British Columbia
AND
D. ROUTLEDGE
Electrical Engineering Department, University of Alberta, Edmonton
Received 1986 August 7; accepted 1986 October 6

ABSTRACT

Radio continuum observations are presented of the supernova remnant (SNR) VRO 42.05.01 (G166.0+4.3). Angular resolution is $\sim 20''$ at 1.4 GHz. Our earlier model of this unusual SNR is elaborated. The model depicts the SNR breaking out from a warm medium of intermediate density, in which the supernova occurred, into a hot, tenuous interstellar cavity, presumably formed by one or more previous supernovae or stellar winds. This model is now shown to be quantitatively consistent with hydrodynamical calculations of an SNR breaking out of a cloud. The SNR has reenergized a section of the hot cavity of extent ~ 120 pc. The interface between the warm medium and the hot cavity has been excited into emission around the breakthrough point. It is argued that the linear features, of width 1 pc and length ~ 80 pc, which are seen crossing the SNR, are regions of this interface where the line of sight is tangential to the surface.

Subject headings: nebulae individual — nebulae: supernova remnants

I. INTRODUCTION

The supernova remnant (SNR) VRO 42.05.01 (G166.0+4.3) was mapped in the radio continuum at 1.4 GHz by Landecker *et al.* (1982, hereafter Paper I). Further investigations of the morphology of the SNR were made by Pineault *et al.* (1985, hereafter Paper II) on the basis of optical line photographs and higher resolution radio maps. In Paper I, it was suggested that the unusual morphology of the SNR is the result of an abrupt density discontinuity in the interstellar medium into which the remnant is expanding. In Paper II, a model was proposed along these lines. In this paper, we present an improved radio map and further examine physical conditions in the environs of the SNR, paying particular attention to the linear features which are seen.

Our model of Paper II depicted the SNR as breaking out from a warm region of intermediate density, across an abrupt boundary into a hot low-density region. Similar situations have been treated quantitatively in recent hydrodynamical calculations by Falle and Garlick (1982) and Tenorio-Tagle, Bodenheimer, and Yorke (1985). Both these studies contain detailed numerical simulations of a SNR expanding across a density discontinuity. Falle and Garlick showed that such a model could quantitatively account for the observed features of the Cygnus Loop, whereas Tenorio-Tagle *et al.* were concerned with following the interaction of SNRs with dense molecular clouds. A result of particular interest common to both studies is an empirical relationship between the density contrast and the ratio of velocities into and away from the dense medium after breakout. We use the results of these two studies to give quantitative support to our model.

II. OBSERVATION AND DATA REDUCTION

The observations were obtained with the Synthesis Telescope at the Dominion Radio Astrophysical Observatory (DRAO) and with the Very Large Array (VLA) of the National Radio Astronomy Observatory.[1] The observations are summarized in Table 1.

The DRAO Synthesis Telescope (Roger *et al.* 1973) employs four 9 m antennas on a 600 m east-west baseline. For continuum mapping at 1.4 GHz, left-hand circularly polarized radiation is received from a 20 MHz band from which the central 5 MHz, centered on the H I line, is excised by a filter. H I radiation is simultaneously processed through a separate correlation system; H I data from observation No. 2 (see Table 1) will be presented in a subsequent paper. Continuum observations were calibrated in amplitude and phase using the sources 3C 147, 3C 295, and 3C 48, using flux densities from Baars *et al.* (1977). The two sets of DRAO observations were separately reduced to maps with angular resolution $1' \times 1'.4$ (east-west × north-south), CLEANed, and averaged to reduce noise.

The 1.45 GHz VLA data from two overlapping fields of diameter 30′ were reduced using natural weighting of the (u, v)-plane to obtain maximum sensitivity to extended structure. Only maps in Stokes parameter I will be presented. Maps in other Stokes parameters were computed, but no significant polarization was observed.

The ultimate aim of the data reduction was to combine the VLA and DRAO data and to add to them data for baselines shorter than 13 m so that the final image represents all baselines from 0 to 3.3 km. Data for baselines shorter than 13 m were derived from a 1.4 GHz map made with the Effelsberg 100 m radio telescope (W. Reich, private communication). The maps were corrected for the response of the primary beam of the antennas (FWHM 105′ Gaussian for DRAO, 30′ Gaussian for the VLA). All the sets of data were then transformed to the

[1] The National Radio Astronomy Observatory is operated by Associated Universities, Inc., under contract with the National Science Foundation.

TABLE 1

Radio Observations of VRO 42.05.01

Date	Telescope	Frequency (MHz)	Baselines (m)	Antenna Beam FWHM	Synthesized Field	Field Centers (1950.0)	
1. 1981 Nov	DRAO	1420	13–600	105′	128′ × 128′	$5^h22^m48^s$	42°52′15″
2. 1982 Oct	DRAO	1420	13–600	105	128 × 128	5 22 48	42 52 15
3. 1983 Mar	VLA (C Config)	1450	65–3300	30	51 × 51	5 22 30	43 09 00
						5 23 00	42 48 00
4.		5000	65–3300	10	...	5 23 00	42 51 48

(u, v)-plane, appropriately filtered, and added. Separate additions were made for each of the two VLA fields, and the two maps were then combined onto a common grid. The resultant beamwidth is 20″ × 16″ (at a position angle of 82°).

III. OBSERVATIONAL RESULTS

Figure 1 shows the map of VRO 42.05.01 in gray-scale representation. Because of the corrections applied for primary beam attenuation, the noise level of the map rises towards the edges of the two VLA observing fields. Low-level sidelobes are evident around a few strong small-diameter sources in the map. The first sidelobe is at −2% and the second at +1%. Their effect on low-level structure is unimportant at distances more than a few beamwidths from the strong sources.

In referring to the parts of VRO 42.05.01, we employ the nomenclature adopted in Papers I and II. The circular shell in the east we refer to as the shell component; the larger limb-brightened structure in the west we refer to as the wing component. With the improvement in angular resolution and sensitivity over the observations of Paper I, several new features of the SNR become apparent. New detail is seen on the shell; its appearance suggests braided filaments. This is most easily interpreted as a surface spherical in grand design but indented in detail. There is less evidence of this on the wing component; the emission inside it is smooth with the maximum brightness at the western edge. The quasi-linear filaments which dominate the east side of the wing and pass through the shell have now been resolved. Their width is ~1′.5 and their length is up to 1°. They can now be clearly traced across the limb of the shell component. From a comparison of the radio map of Figure 1 and the Hα image (Fig. 2 of Paper II) we see that most of these radio-emitting filaments also emit optically. The strong resemblance between many of the radio features and the optical emission was remarked on in Paper II.

The linear filaments appear to be quite smooth. The apparent condensation seen in the northern filament in the map of Paper I is now seen to be an unresolved source. It is probably extragalactic.

The "break" in the western edge of the wing is now a little better resolved, but the southern extremity of the wing disappears into the noise and is no better delimited by the new observations. In the north, the end of the wing is again lost in the noise, but some new details are apparent. The straight filaments on the eastern side extend even beyond the bright western edge of the wing.

IV. THE MODEL

In Paper II, we presented a model for the evolution of VRO 42.05.01 in a multicomponent interstellar medium (ISM), paying particular attention to the large-scale aspects of this evolution. The essential features of this model are depicted in Figure 2. S, the shell component of the SNR, marks the shock front expanding in the warm medium of intermediate density in which the SNR explosion occurred (the upper slab). The shock has broken out of the upper slab, across an abrupt density discontinuity, into a hot, low-density cavity (the tunnel). The shock has crossed the tunnel and has encountered another slab of material of intermediate density (the lower slab) and the wing component W has formed as a result. The hot, low-density region has been referred to as a "tunnel" following the hypothesis of Cox and Smith (1974), who suggested that cavities which form in the ISM as the result of supernovae and stellar winds amalgamate to become an interconnecting system of tunnels. Here we present a quantitative treatment of the breakout process and the subsequent reenergization of the tunnel. We interpret the linear features as one of the consequences of that reenergization and consider them to lie on the boundary between the upper slab and the tunnel.

Although the model of Figure 2 assumes a plane interface, this surface is unlikely to be plane and may well be twisted. The fact that the linear features in Fig. 1 are not parallel, and in fact sometimes intersect or bifurcate, supports this. In Figure 2, the width of the hot tunnel has been exaggerated for clarity, and the model is depicted in perspective although the line of sight to the real object is approximately parallel to the surfaces of the slabs.

a) General Discussion of Tunnel Reenergization

The sequence of events envisaged in our model is depicted in Figure 3. As the supernova blast wave breaks out from the relatively dense medium in which it occurred, it reenergizes the tunnel, as Smith (1977) suggested. It seems immaterial whether the hot tunnel is the product of previous supernova events, the situation described by Smith, or of stellar wind bubbles (Castor, McCray, and Weaver 1975; McKeee, van Buren, and Lazareff 1984); both causes lead to the same conditions within the tunnel and at its walls.

We assume that the walls of the hot tunnel would not have been detectable by radio or optical observations before the supernova breakout. Our model proposes that the shock breaking into the hot tunnel, as well as reenergizing the interior of the tunnel, has excited a large area of the interface into emission around the breakthrough point. The linear features are emitting regions in the interface where the line of sight is tangential to the surface. In other words, we are seeing corrugations in that surface, and the linear features are made visible by enhancement of optical depth. The corrugations may have arisen as Rayleigh-Taylor instabilities in the interface. The magnetic field, which we assume is aligned with the long dimension of the tunnel and roughly perpendicular to the line of sight, will stabilize the interface against such perturbations in the direction parallel to the field (Kruskal and Schwarzschild 1954). The field direction could be assessed by measure-

1987ApJ...315..580P

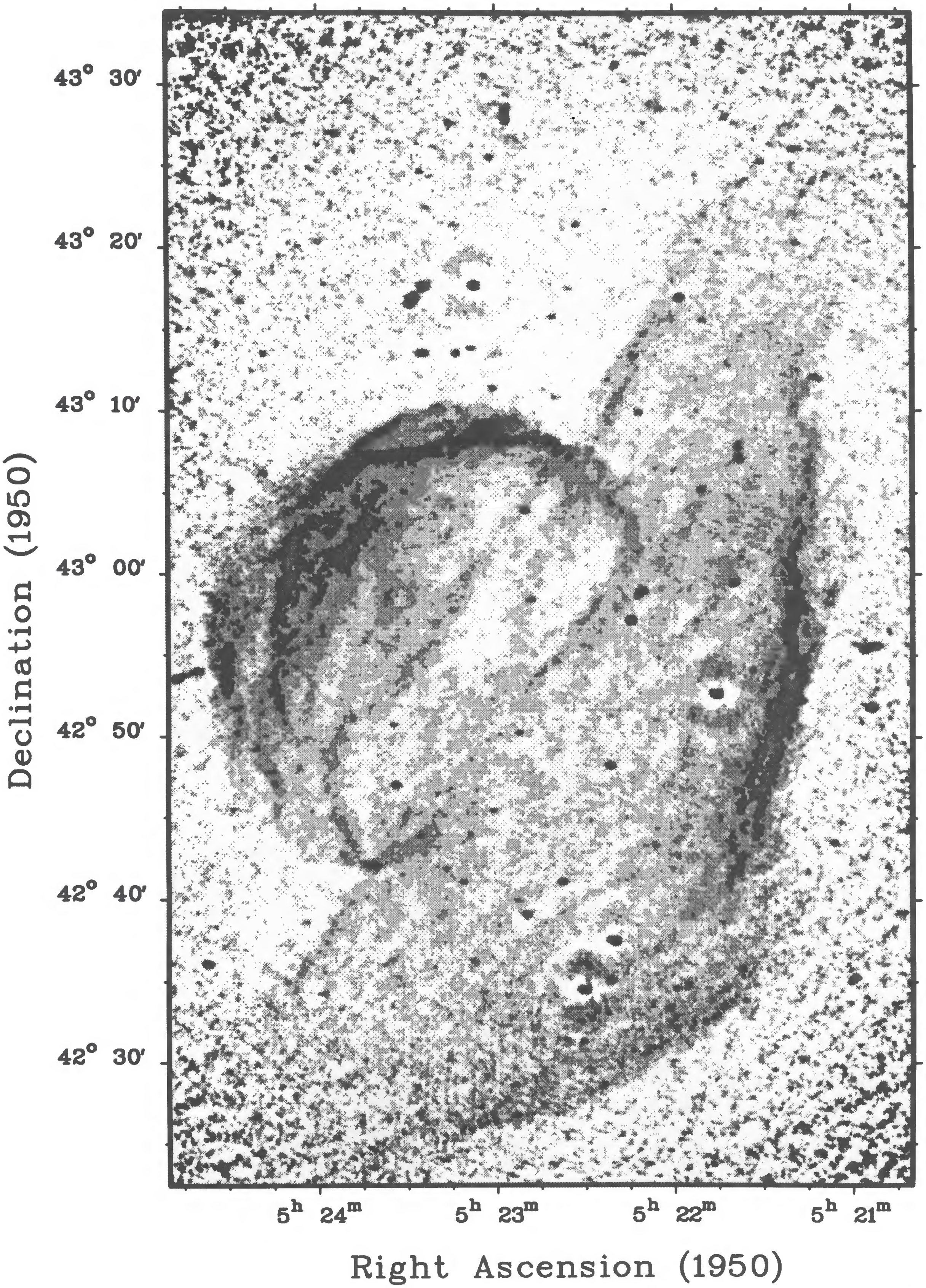

FIG. 1—Gray-scale representation of the 1.4 GHz continuum emission from VRO 42.05.01 (G166.0+4.3). The map is the combination of data obtained from the 100 m Effelsberg telescope, the DRAO Synthesis Telescope, and the VLA in the C configuration. All baselines from 0 to 3300 m are present. The beamwidth is 16″ × 20″ at P.A. 82°.

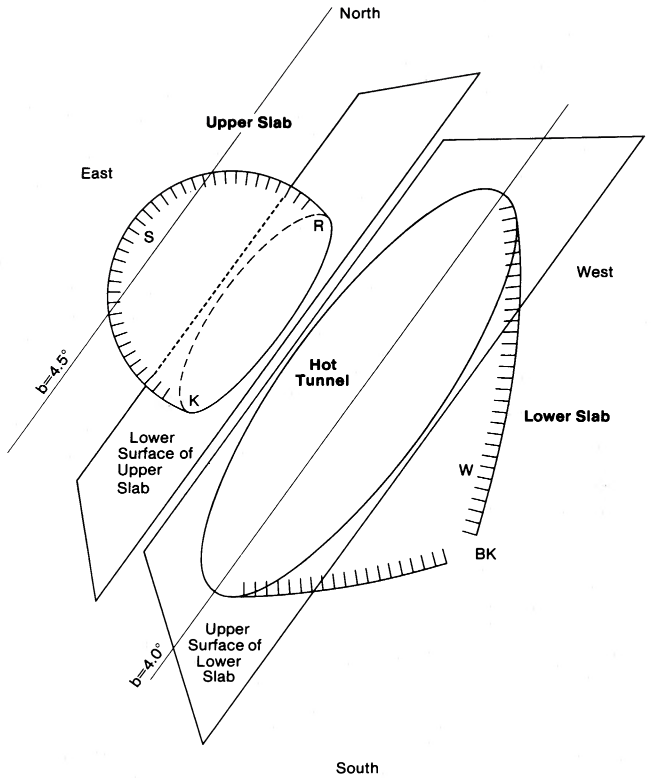

FIG. 2.—Schematic diagram depicting the various features of VRO 42.05.01. The linear or quasi-linear features which are believed to outline the boundary of the hot tunnel are assumed to lie on the lower surface of the upper slab.

ments of the polarization of the radio emission from the linear filaments, although very high sensitivity would be required.

The relative straightness of the filaments needs some explanation. While SNRs and stellar winds usually generate spherical cavities, when such cavities amalgamate in the manner envisaged by Cox and Smith (1974), the tension in the magnetic flux tubes in the walls will tend in time to straighten those walls.

Because of compression by previous supernovae or stellar winds, the density and magnetic field in the tunnel walls will exceed those of the undisturbed warm medium, and we expect the field to be reasonably well ordered parallel to the walls. In keeping with the notation used in Paper II, the subscripts "h" and "w" refer respectively to the undisturbed hot tunnel and the warm slabs. If we let x_+ (subscript "$+$" for wall parameters) denote the residual compression factor of the tunnel walls, then $\rho_+ = x_+ \rho_w$ and, by conservation of magnetic flux in the one-dimensional compression across a shock, $B_+ = x_+ B_w$. An upper limit on B_+ of 6×10^{-6} G is obtained if we assume that the magnetic pressure in the walls balances the kinetic pressure of the hot tunnel.

For convenience, the adopted parameters are summarized in Table 2 together with the derived evolutionary history of the SNR. The current shock radius of the shell is 25 pc, based on a distance to the SNR of 5 kpc (derived from Σ-d considerations; see Paper I for details). In a cloudy ISM (e.g., Blandford and Cowie 1982), the warm slabs are assumed to contain cool, dense clouds which, when crushed by the SNR blast wave, give rise to the observed radio and optical emission.

In Paper II, we estimated the age of the SNR to be $\sim$55,000

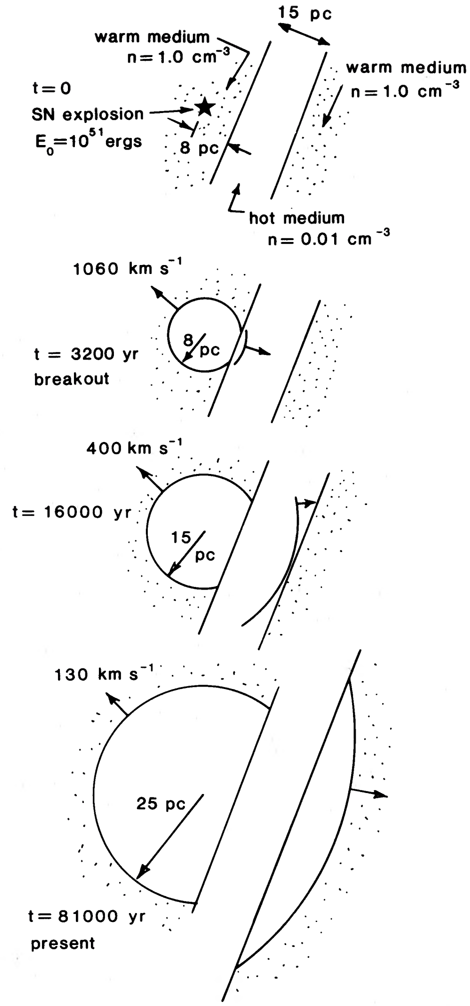

FIG. 3.—Schematic diagram showing four stages in the evolution of VRO 42.05.01 in the multicomponent medium surrounding it. Various numerical values are based on data from Tables 2 and 3. A tunnel width of 15 pc has been adopted. Velocities shown are shock velocities. See text for a discussion of the velocity in the wall opposite the breakout point (the wing component).

TABLE 2

ADOPTED AND DERIVED MODEL PARAMETERS

Warm slabs:	
Hydrogen number density n_w	1 cm^{-3}
Temperature T_w	10^4 K
Hot tunnel:	
Hydrogen number density n_h	0.01 cm^{-3}
Temperature T_h	10^6 K
Distance to SNR	5 kpc
Supernova evolution:	
Total energy E_0	10^{51} ergs
Breakout parameters:	
Time t_b	3200 yr
Shell radius R_b	8 pc
Shell shock velocity v_b	1060 km s^{-1}
Transition parameters from adiabatic to isothermal phase:	
Time t_*	29400 yr
Shell radius R_*	19.4 pc
Shell shock velocity v_*	280 km s^{-1}
Current parameters:	
Age t_0	81000 yr
Shell radius R_0	25 pc
Shell shock velocity v_0	130 km s^{-1}

yr on the assumption of uninterrupted adiabatic evolution. However, our choice of parameters implies that the temperature behind the shock falls below 10^6 K after $\sim 29{,}000$ yr, at which time cooling becomes important. This transition from adiabatic ($R \propto t^{2/5}$) to isothermal ($R \propto t^{1/4}$) evolution (see, e.g., Spitzer 1978 for a review) has been taken into account in deriving the age shown in Table 2. The precise form of the evolutionary law affects time scales but is not expected to alter our main conclusions concerning the morphology of the remnant. A slightly lower slab density, $n_w = 0.5$ cm^{-3}, would have resulted in continuous adiabatic evolution throughout, and a correspondingly lower age for the SNR.

Before considering in detail the effect of shocks propagating along the tunnel and into the walls, we ask whether particles which have been shock-accelerated before breakout could adequately explain the radio linear features delineating the boundary of the upper slab. This would require that relativistic particles, after injection into the tunnel, have propagated sufficiently far, both along and into the walls, to account for the observed extent of the linear features. However, the streaming velocity of the relativistic particles is only similar to or somewhat larger than the Alfvén velocity v_A (Wentzel 1974; Cesarsky 1980), where

$$v_A = B/(4\pi\rho)^{1/2} \approx 2 \text{ km s}^{-1}(B/10^{-6} \text{ G})n^{-1/2} . \quad (1)$$

Even in the very tenuous hot tunnel this velocity is too small, compared to the shock velocity of the shell, to be of any importance. Further, any relativistic particle finding itself free to stream away into the hot tunnel would only be able to penetrate the walls a distance of about its Larmor radius r_L, where

$$r_L \approx 10^{-5} \text{ pc } (v/1.4 \text{ GHz})^{1/2}(B/10^{-6} \text{ G})^{-3/2} . \quad (2)$$

This is clearly far too small to account for the observed width of the linear radio features, which is ~ 1 pc. Furthermore, ionizing photons must be available to excite the observed optical line emission (Paper II; Fesen, Gull, and Ketelsen 1983; Parker, Gull, and Kirshner 1979).

For the walls to emit both radio and optical radiation over the observed area, there must therefore be an additional and important source of relativistic particles and excitation, over and above the simple injection of previously accelerated particles. The shock driven along the tunnel and then into its walls by the newly increased interior pressure is such a source.

Consider first the wall opposite breakout (the west side of the wing). From the parameters listed in Table 2, we deduce that 50 $M_\odot$ of material has been swept up by the time breakout occurs. About half of this will be dumped into the tunnel. This matter will consist of a mixture of hot gas and crushed clouds filled with freshly accelerated radio-emitting electrons (Blandford and Cowie 1982). Although most of these clouds may have evaporated either in the ambient postshock medium or in the hot tunnel, we may expect the densest and largest clouds to survive evaporation (Cowie and McKee 1977) and to cross the tunnel. For this reason, and because of the breakout geometry, the wall diametrically opposite the breakthrough point should show considerably more radio and optical emission, and indeed this explains both the level of emission and the general shape of the wing component, as suggested in Paper II.

b) Quantitative Model of Tunnel Reenergization

We now discuss the emission from the parts of the wall adjacent to breakout and the diffuse radio emission filling the volume east of the wing component and show in detail that these features are quantitatively consistent with the cavity rejuvenation hypothesis of Cox and Smith (1974) and Smith (1977).

As a result of the increased pressure in the tunnel following breakout, an adiabatic shock wave propagates along the tunnel driving isothermal shocks into the much denser tunnel walls. Given the conditions summarized in Table 2, we are interested in finding out how far, at any given time, the tunnel shock will have progressed and what the shock velocity in the wall will be. Remembering that the spherically symmetric adiabatic solution yields a shock velocity

$$v \propto \frac{(E_i)^{1/2}}{\rho V} , \quad (3)$$

where E_i, V, and ρ are the internal energy, interior volume, and density ahead of the front (Spitzer 1978), we expect the shock wave to accelerate as it enters the much lower density tunnel and, as the interior volume increases, to decelerate eventually. We also expect the velocity u of the material behind the shock to exhibit the same general behavior. In the following discussion we use the letters "v" and "u" to denote shock and material velocities respectively. For an adiabatic shock, characterized by a compression factor of 4, $u = 0.75v$.

The recent numerical studies of Falle and Garlick (1982) and Tenorio-Tagle, Bodenheimer, and Yorke (1985) confirm the general picture sketched above. The growth of the shock velocity through the breakout process is difficult to predict and depends on both the contrast in density and the distance of the explosion from the discontinuity. However, Tenorio-Tagle *et al.* obtain a result which we can use to predict the final velocity of material that has broken out of the slab. Along the symmetry axis (normal to the surface of the slab at the breakthrough point), B is the ratio of the velocity of the material breaking *out of* the slab to the velocity of material on the other side of the SNR shell which continues to expand *into* the slab. These authors show that B eventually reaches a constant value which depends only on the density contrast $\lambda = n_h/n_w$. For the case of adiabatic evolution, they obtain the empirical result

$$B_\infty = 4.22 - 1.89(\log \lambda + 2) . \quad (4)$$

This relation allows us to predict the evolution of the SNR after breakout, as long as we know the inward shell velocity u_s. Using the adiabatic solution for the material velocity of the shell component, we have

$$u_s = \tfrac{3}{4}v_s = \tfrac{3}{4}v_b \tau^{-3/5} , \quad (5)$$

where v_b is the shock velocity of the shell at breakout (Table 2) and $\tau = t/t_b$. Both Falle and Garlick (1982) and Tenorio-Tagle, Bodenheimer, and Yorke (1985) have shown that, to a high degree of accuracy, the part of the SNR in the denser medium continues to evolve as if breakout had not occurred. In other words, it is as if the two parts of the SNR did not know about each other. Therefore we can calculate the inward velocity using standard adiabatic or isothermal models.

In equation (5) we have used the adiabatic solution, despite the fact that we concluded above that the evolution ceases to be adiabatic after $\sim 29{,}000$ yr. Therefore equation (5) will give an overestimate of the distance traveled. Furthermore, because equation (4) applies to motion along the symmetry axis, it represents the maximum material velocity achieved, and its use to estimate the lateral distance propagated along the tunnel, in roughly northwest and southeast directions, will also lead to an overestimate irrespective of whether transition to isothermal evolution takes place or not.

Before we proceed to evaluate propagation along the tunnel, we should note that equation (4) is valid only for large values of τ, i.e., $\tau \geq 5$. To take into account the initial acceleration phase following breakout, we have considered Figure 2 of Falle and Garlick (1982), which shows the time-dependent behavior of the ratio B. We find that a remarkably good fit is obtained if we let

$$B(\tau) = B_\infty - (B_\infty - 1)/\tau \,, \tag{6}$$

where B_∞ is the limiting value of $B(\tau)$ at large τ. This obviously reduces to the correct values for the limits $\tau \to 1$ and $\tau \to \infty$. Assuming the hot interior of the broken-out remnant to be delimited by the position of the outward-moving density maximum, we obtain the following two expressions for the evolution of the maximum material velocity $u_{\max}$ and distance $D_{\max}$ propagated down the tunnel:

$$u_{\max} = \tfrac{3}{4} v_b \tau^{-3/5}[B_\infty - (B_\infty - 1)/\tau] \,, \tag{7}$$

$$\begin{aligned} D_{\max} &= \int_{t_b}^{t} u_{\max}\, dt = t_b \int_1^\tau u_{\max}\, d\tau \\ &= \tfrac{5}{8} v_b t_b [3B_\infty \tau^{2/5} + 2(B_\infty - 1)\tau^{-3/5} - (5B_\infty - 2)] \,. \end{aligned} \tag{8}$$

Finally, we estimate the velocity of the shock driven into the tunnel walls by scaling according to the density increase encountered when going from the tunnel interior back into the slabs. Assuming that the shock and material velocities in the hot interior obey the usual adiabatic relation for a compression ratio of 4, we obtain, by simply matching shock velocities at the interface.

$$u_{\rm wall} = v_{\rm wall} = \tfrac{4}{3} u_{\max}(x_+ n_w/n_h)^{-1/2} \,, \tag{9}$$

where x_+ denotes the residual compression factor (subscripts "wall" and "+" are equivalent). Because of the much higher density of the slabs, the shocks in the walls are isothermal, and shock and material velocities are equal. For reasons already mentioned, equation (9) should be considered as an upper limit to the velocity in the walls.

Table 3 summarizes the results of the model. Each line shows, for a given dimensionless time τ, the instantaneous radius R_s of the shock associated with the shell, the maximum tunnel material velocity $u_{\max}$, the maximum distance $D_{\max}$ traveled along the tunnel, and the wall velocity $u_{\rm wall}$ for three plausible values of the residual compression factor x_+. The last line reflects the current conditions for the choice of parameters shown in Table 2. Because of the many uncertainties and assumptions underlying the analysis, we believe that the good agreement between the observed extent of the linear emission to the northwest and southeast (~60 pc for an assumed distance of 5 kpc to the SNR), and the calculated value of $D_{\max}$ shows the consistency of the proposed model. We note that the observed extents of the linear features in the northwest and southeast directions are nearly equal, and this provides additional support for our model.

TABLE 3

MODEL EVOLUTIONARY HISTORY

τ	R_s (pc)	$u_{\max}$ (km s^{-1})	$D_{\max}$ (pc)	$u_{\rm wall}$ (km s^{-1}) $x_+ = 1$	$x_+ = 2$	$x_+ = 5$
4	13.9	1180	12	158	111	70
8	18.4	870	25	116	82	52
12	20.7	710	36	94	67	42
16	22.3	610	44	81	57	36
20	23.6	530	52	71	50	32
24	24.7	480	58	64	46	29
25.3	25.0	470	60	62	44	28

We also see from Table 3 that the tunnel should be crossed in a relatively short time. It is difficult to estimate accurately the width of the tunnel before breakout; however, if we consider a tunnel width of 15 pc, as assumed in Figure 3, then the matter which breaks out and reaches the opposite side of the tunnel after ~16,000 yr ($\tau \approx 5$), at which time an isothermal shock is driven into this wall with initial shock velocity $u_{\rm wall}$. The current shock velocity of the wing component depends on the actual width of the tunnel, because this distance determines the initial shock velocity in the wall. However, it is expected and easily verified that the current shock velocity of the wing component should be similar to or somewhat smaller than the tabulated value of $u_{\rm wall}$, i.e., ~60 km s^{-1} for $x_+ = 1$. This compares with the estimated current shock velocity of 130 km s^{-1} for the shell component.

An alternative approach to the empirical analysis we have just presented is to follow analytically the adiabatic expansion of the combined volume consisting of the shell component plus the tunnel. This requires an assumption about the shape of the tunnel, on which we have very little information. For example, we might consider the tunnel to be a cylindrical tube of fixed diameter and allow expansion only along the tube. Another possibility is to consider the tunnel as having two plane walls which are parallel with fixed separation and allow free expansion between these walls. Both these situations are amenable to calculation by numerical integration of equation (3) from a time just after breakout. The interior volume V undergoing adiabatic expansion now includes the spherical volume behind the shell and the increasing volume in the tunnel.

To make such calculations we must know the velocity with which material breaks through the interface into the tunnel. It is clear that the material will accelerate upon breakout, but how much and for how long? The flow following breakout will be hydrodynamically complex, and energy will be shared between internal and kinetic energies. Nevertheless, it is possible to obtain a reasonable estimate of the peak material velocity $u_{\rm peak}$ in the tunnel just after breakout and of the duration Δt of the acceleration phase. A crude density scaling argument (Spitzer 1978) would predict a tunnel shock velocity just after breakout on the order of 10,600 km s^{-1}, yielding a material velocity of ~8000 km s^{-1} (assuming the customary adiabatic relation $u = 0.75v$). However, the matter just injected into the tunnel cannot reach such a high velocity, as can be seen from the following simple argument. Consider that the entire hemispherical shell of radius R_b and mass M_b breaks out into the tunnel at t_b. Assuming that half the supernova energy is available to accelerate it, we have

$$0.5E = \frac{1}{2} M_b u_{\rm peak}^2 = \frac{\pi}{3} \rho_w R_b^3 u_{\rm peak}^2 \,, \tag{10}$$

from which we deduce that $u_{\rm peak} = 1400$ km s^{-1}. From Figure 1, we estimate an increase in the volume by a factor of ~10 between breakout and the present time so that, for adiabatic evolution, we should expect a current material velocity in the tunnel of ~1400 km s$^{-1}/\sqrt{10} \approx 440$ km s^{-1}.

The duration Δt of the acceleration phase can also be estimated. Because the pressure in the tunnel is negligible compared to that inside the expanding shell, the accelerating force at breakout should be roughly Ap, where A and p are respectively the area of the hemispherical shell and the inside pressure $p \approx E/2\pi R_b^3$ (Spitzer 1978). On dimensional grounds, the acceleration is of order $u_{\rm peak}/\Delta t$, from which we obtain

$$\Delta t \approx M_b u_{\rm peak} R_b/E . \tag{11}$$

The duration of the acceleration phase is thus $\Delta t \approx 5800$ yr.

Taking 1400 km s^{-1} as the shock velocity in the tunnel immediately after breakout, we calculated the progress of adiabatic expansion in the tunnel using both geometries described above. The results are surprisingly similar, suggesting that the exact shape of the tunnel is unimportant. The results give material velocities, and therefore distances along the tunnel, of about half the values given in Table 3. Since we have emphasized that the method used to derive the values given in Table 3 is likely to yield an overestimate, this agreement is satisfactory, considering the imprecision of our knowledge of the initial shock velocity in the tunnel.

We find surprisingly good agreement between some of the empirical results of Table 3 and the analytical estimates we have just derived. For example, the last line of Table 3 shows the current material velocity at the ends of the tunnel to be 470 km s^{-1}, very close indeed to our estimate of 440 km s^{-1}, based on a volume expansion factor of 10. By differentiating equation (7), we find the time of peak velocity of material in the tunnel is $t = 6500$ yr, when the velocity is 1370 km s^{-1}. Our analytical estimates corresponded to a time of 9000 yr (5800 + 3200) and a velocity of ~ 1400 km s^{-1}.

Table 3 also brings out the fact that two factors will generally determine the actual extent of any radio or optical emission emanating from reenergized tunnel walls. These are the time, and consequently the distance traveled since breakout, and the velocity of the shock triggered in the wall. For it is clear that, even if an increasing fraction of tunnel volume is being rejuvenated, a point will be reached where shocks in the walls are too weak to produce a significant emission. This is becoming apparent in Table 3 for the case $x_+ = 5$. In principle, this should lead to an observable gradient in optical line ratios. Unfortunately, the observations reported in Paper II are not of sufficient sensitivity and do not cover enough tunnel area to provide any data of this sort.

A related question concerns the extent to which other aspects of the optical morphology of the remnant can be explained by the model which we propose. Particularly striking is the fact that, whereas the entire wing component is clearly visible in Hα + [N II] line photographs, the northern part is totally absent in the light of [O III] (Fesen, Gull, and Ketelsen 1983), as are the linear filaments. Similar morphological differences have also been noted for other SNRs, for example the Cygnus Loop (Fesen, Blair, and Kirshner 1982) and IC 443 (Fesen and Kirshner 1980). Because the [N II] lines are formed in cooler regions than the [O III] lines, Fesen, Gull, and Ketelsen (1983) have suggested that the morphological differences are due to an inhomogenous interstellar medium. In this picture, the northern part of the wing component is required to have a higher mean density, leading to a lower post-shock temperature and hence less [O III] emission. This seems reasonable, since the correspondingly lower shock speed then implies that the blast wave has traveled a shorter distance into the lower slab (as compared to the southern part of the wing component), just as our radio observations seem to suggest.

A final question concerns the apparent symmetry and completeness of the eastern hemispherical shell, which might seem unexpected for an 80,000 yr old SNR. We note that the ages we have derived could be significantly lower if the density in the warm slab were smaller than that adopted in our model calculations. A density of 0.5 cm^{-3}, half as large as the one we used, would result in adiabatic evolution approximately to the present time and consequently an age of some 40,000 yr.

V. ALTERNATIVE HYPOTHESES

SS 433 is probably the best case of a SNR where jets of relativistic particles are observed (Margon, Grandi, and Downes 1980). Another Galactic source, Sco X-1 (e.g., Fomalont *et al.* 1983), exhibits a structure reminiscent of extragalactic double radio sources, which are believed to be powered by beams of energetic particles. Manchester and Durdin (1983) and Gregory and Fahlman (1983) have also hypothesized that the structure of some SNRs may be shaped by the interaction of beams with the surrounding medium. Could some of the features of VRO 42.05.01 be linked to the activity of a compact stellar remnant?

As our first radio map (Paper I) did weakly suggest such a possibility, we undertook to search for evidence of a compact remnant near the center of the shell component. As reported previously (Paper II), an optical search failed to turn up a candidate. Our best 1.4 GHz radio continuum map, Figure 1, clearly does not show any point source or evidence of central linear structures on small scales. Similarly no suggestive source or structure could be seen on the 5 GHz VLA map.

R. N. Henriksen (private communication) has suggested that the wing component of VRO 42.05.01 shows a resemblance to a recently proposed new class of axisymmetric radio sources (Becker and Helfand 1985; Helfand and Becker 1985), G5.3 − 1.0 being the closest analog to VRO 42.05.01. In Becker and Helfand's model, jets of energetic particles are produced by a high-velocity accreting binary system. Their model, applied to the wing component of VRO 42.05.01, would predict the presence of a compact binary somewhere near the "break" in the wing component (approximate coordinates $\alpha \approx 5^{\rm h}21^{\rm m}.5$, $\delta \approx 42°40'$). If this postulated object were assumed to be the compact remnant of the supernova explosion responsible for the shell component, it would have had to travel a distance of ~ 50 pc in 81,000 yr, corresponding to a velocity of ~ 600 km s^{-1}. This large velocity, and the fact that this model alone fails to explain the linear features, make it doubtful that the wing component is a member of this new class of objects.

VI. CONCLUSION

We believe that VRO 42.05.01 represents one of the best examples to date of a SNR breaking out into a hot tunnel or cavity left either by previous supernovae or stellar wind bubbles, as suggested initially by Cox and Smith (1974). Furthermore, we have found evidence that the cavity has been reenergized over a substantial area near the breakout point of the blast wave.

We are grateful to Dr. W. Reich for permission to use his unpublished data, and we wish to thank R. N. Henriksen for useful discussions. This research was supported by grants to S. P. and D. R. from the Natural Sciences and Engineering Research Council of Canada. The DRAO Synthesis Telescope is operated as a national facility by the National Research Council of Canada.

REFERENCES

Baars, J. W. M., Genzel, R., Pauliny-Toth, I. I. K., and Witzel, A. 1977, *Astr. Ap.*, **61**, 99.
Becker, R. H., and Helfand, D. J. 1985, *Nature*, **313**, 115.
Blandford, R. D., and Cowie, L. L. 1982, *Ap. J.*, **260**, 625.
Castor, J., McCray, R., and Weaver, R. 1975, *Ap. J. (Letters)*, **200**, L107.
Cesarsky, C. J. 1980, *Ann. Rev. Astr. Ap.*, **18**, 289.
Cowie, L. L., and McKee, C. F. 1977, *Ap. J.*, **211**, 135.
Cox, D. P., and Smith, B. W. 1974, *Ap. J. (Letters)*, **189**, L105.
Falle, S. A. E. G., and Garlick, A. R. 1982, *M.N.R.A.S.*, **201**, 635.
Fesen, R. A., Blair, W. P., and Kirshner, R. P. 1982, *Ap. J.*, **262**, 171.
Fesen, R. A., Gull, T. R., and Ketelsen, D. A. 1983, *Ap. J. Suppl.*, **51**, 337.
Fesen, R. A., and Kirshner, R. P. 1980, *Ap. J.*, **242**, 1023.
Fomalont, E. B., Geldzahler, B. J., Hjellming, R. M., and Wade, C. M. 1983, *Ap. J.*, **275**, 802.
Gregory, P. C., and Fahlman, G. G. 1983, in *IAU Symposium 101, Supernova Remnants and their X-ray Emission*, ed. J. Danziger and P. Gorenstein (Dordrecht: Reidel), p. 429.
Helfand, D. J., and Becker, R. H. 1985, *Nature*, **313**, 118.
Kruskal, M., and Schwarzschild, M., 1954, *Proc. Roy. Soc. London, A*, **223**, 348.
Landecker, T. L., Pineault, S., Routledge, D., and Vaneldik, J. F. 1982, *Ap. J. (Letters)*, **261**, L41 (Paper I).
Manchester, R. N., and Durdin, J. M. 1983, in *IAU Symposium 101, Supernova Remnants and their X-ray Emission*, ed. J. Danziger and P. Gorenstein (Dordrect: Reidel), p. 421.
Margon, B., Grandi, S. A., and Downes, R. A. 1980, *Ap. J.*, **241**, 306.
McKee, C. F., van Buren, D., and Lazareff, B., 1984, *Ap. J. (Letters)*, **278**, L115.
Parker, R. A., Gull, T. R., and Kirshner, R. P. 1979, *An Emission-line Survey of the Milky Way* (Washington, D.C.: NASA SP-434).
Pineault, S., Pritchet, C. J., Landecker, T. L., Routledge, D., and Vaneldik, J. F. 1985, *Astr. Ap.*, **151**, 52 (Paper II).
Roger, R. S., Costain, C. H., Lacey, J. D., Landecker, T. L., and Bowers, F. K. 1973, *Proc. IEEE*, **61**, 1270.
Smith, B. W. 1977, *Ap. J.*, **211**, 404.
Spitzer, L. 1978, *Physical Processes in the Interstellar Medium* (New York: Wiley), p. 258.
Tenorio-Tagle, G., Bodenheimer, P., and Yorke, H. W. 1985, *Astr. Ap.*, **145**, 70.
Wentzel, D. G. 1974, *Ann. Rev. Astr. Ap.*, **12**, 71.

S. PINEAULT: Département de Physique, Université Laval, Québec G1K 7P4, Canada

T. L. LANDECKER: Dominion Radio Astrophysical Observatory, National Research Council of Canada, Penticton, B.C. V2A 6K3, Canada

D. ROUTLEDGE: Electrical Engineering Department, University of Alberta, Edmonton, Alberta T6G 2G7, Canada